OpticStudio Module 1

CHRIS MAY

*cmay7@uoregon.edu

Abstract: This document includes descriptions of four topics which were explored during the first module of OpticStudio training. The simulation and affects of stop position around a singlet are investigated along with the design of an SLR-type camera lens consisting of a conventional double Gauss. A Young's double slit experiment is investigated and compared to theoretical models of the intensity profile. And a simple design for an Optical Spectrometer is produced from scratch.

1. Singlet RMS Spot Radius

Background

OpticStudio was used to design two models of a lens with $\frac{F}{\#} = 10$. The first lens was designed with a Stop (fixed aperture) before the optic while the second lens had the Stop after the optic. The goal is to determine which lens system has the smallest RMS spot radius and balanced aberrations.

Methods

For both systems, an initial entrance pupil diameter of $40mm$ was specified to allow $588nm$ light through the model lenses at an incident and oblique angle of 5°. Both lenses had boundary conditions for the glass thickness as $3mm \leq t_{glass} \leq 15mm$ with an edge thickness of $3mm$. The thickness of air was allowed to be, $0.5mm \leq t_{air} \leq 1m$ with an edge thickness of $0.5mm$. The optimization function was based on the Spot criterion with the centroid as the reference and Gaussian Quadrature was used to minimize the Merit function. Both materials were N-BK7 so that the geometric characteristics of the lenses were the only variables.

For the lens with the stop before the optic, the surface which was used to determine the $\frac{F}{\#}$ was the rear side of the lens. The variables were the thickness of air between the stop and lens front, the lens front radius and thickness, as well as the thickness of air between the lens rear and the imaging plane.

The lens with the stop after the optic used the location of the Stop to determine the $\frac{F}{\#}$. The variables were the thicknesses of the lens front and rear, as well as the thickness of air between the object-lens front and the stop-imaging plane. The radius of the front lens was also allowed to vary, and the rear lens radius was also allowed to vary but was in the end fixed at infinity due to a large amount of aberration and distortion.

Results

Two fields were applied to the system, one which was incident on the lens and a second that was angled at 5°, the ray diagrams can be seen in Fig. 1. The stop can be seen before the optic in Fig. 1a where the rays begin, and the stop can be seen after the optic in Fig. 1b about 20mm to the right of the last surface of the lens. The ray diagrams are somewhat inconclusive as to whether or not the aperture before or after the optic results in more or less aberration.

A better method for observing the amount of aberration due to stop location is to look at the spot diagrams which are shown in Fig. 2. The spot diagram of the incident field with the stop before the optic has a spot diagram with diameter about $80mm$, and the spot diagram for the stop after the optic for the same field has a diameter of about $200mm$. For the off axis field, both spot

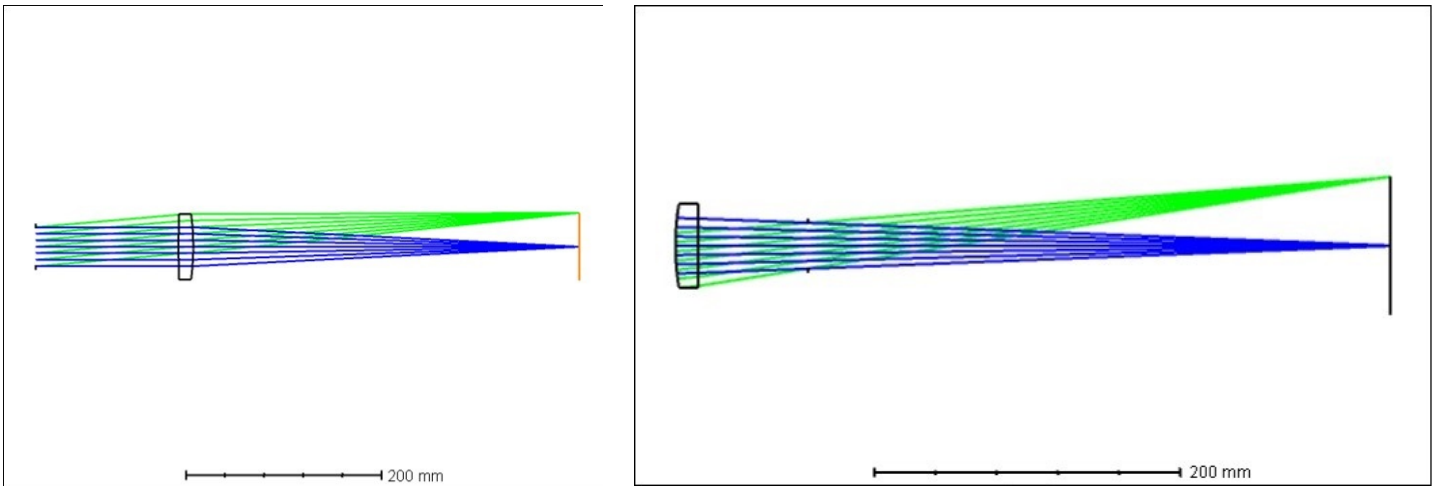

(a) Stop Before Optic (b) Stop After Optic

Fig. 1: Layouts for variations of stop position.

diagrams indicate extrafocal astigmatism but the total amount of astigmatism is much larger for the system where the stop is after the optic. This trend can be seen further when observing the RMS v. Field in Fig. 3 where the system with the stop after the optic has about twice the total spot size for the entire field. Potentially the most definitive method for determining the amount of aberration for the two systems is to take a look at the Seidel coefficients in Fig. 4 which quantify the total aberration of the system. The system with the aperture after the optic has a distortion coefficient which is two units higher than the stop before the optic system.

From this information its safe to say that the position of the stop has a noticeable impact on the amount of aberration which is seen at the imaging screen. It seems that having the stop after the optic causes more dramatic astigmatism and distortion but less spherical aberration than the system with the stop before the optic.

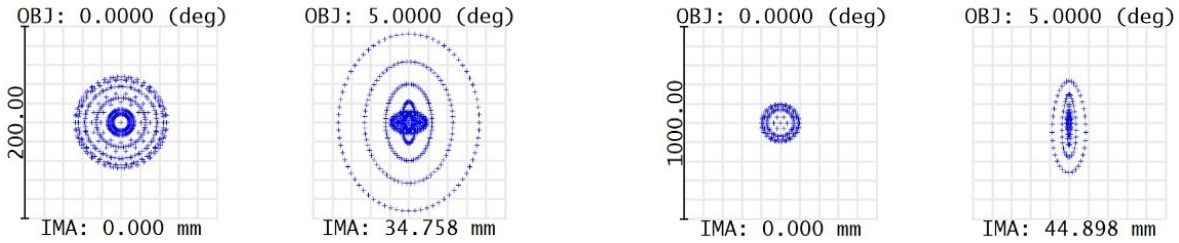

(a) Stop before optic

(b) Stop After Optic

Fig. 2: Spot diagrams for variations of stop position

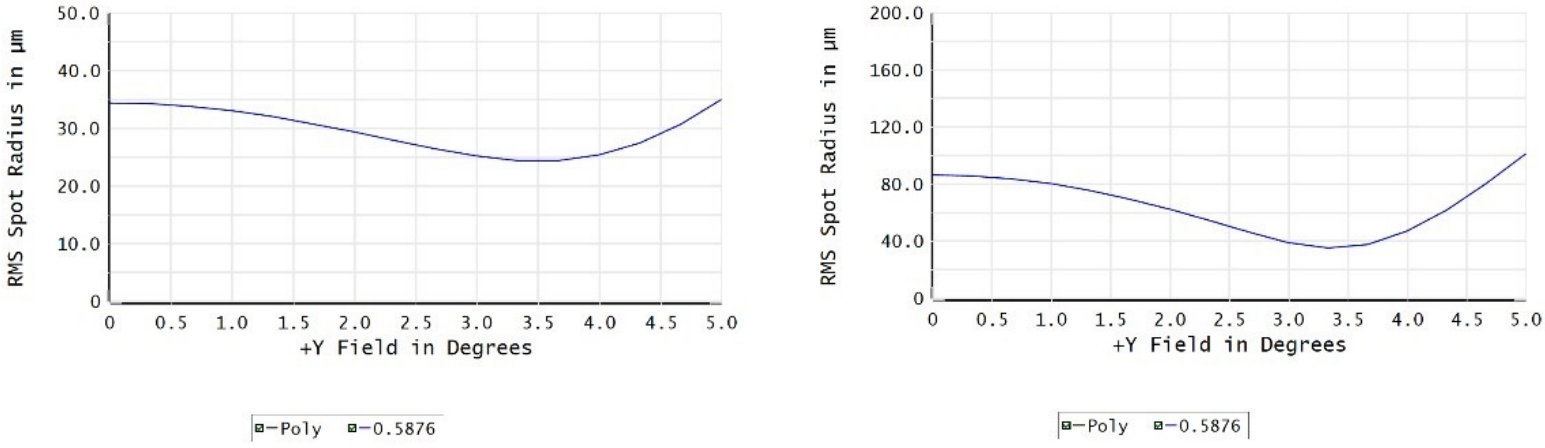

(a) Stop before optic

(b) Stop after optic

Fig. 3: RMS v. Field

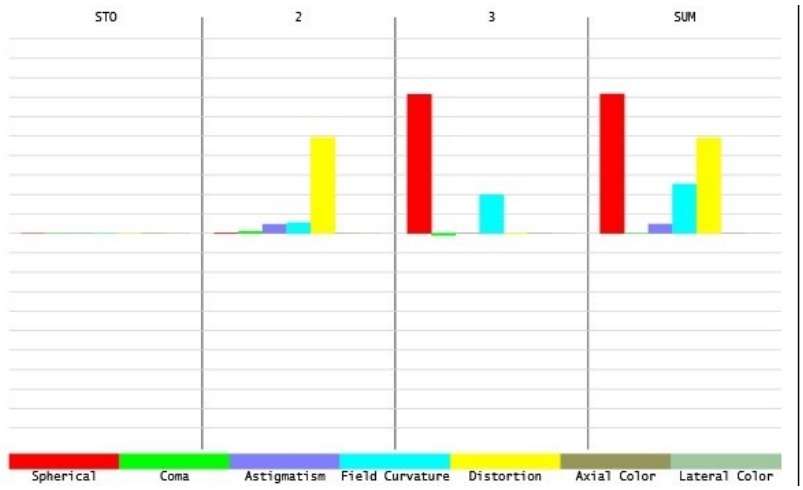

(a) Stop before optic.

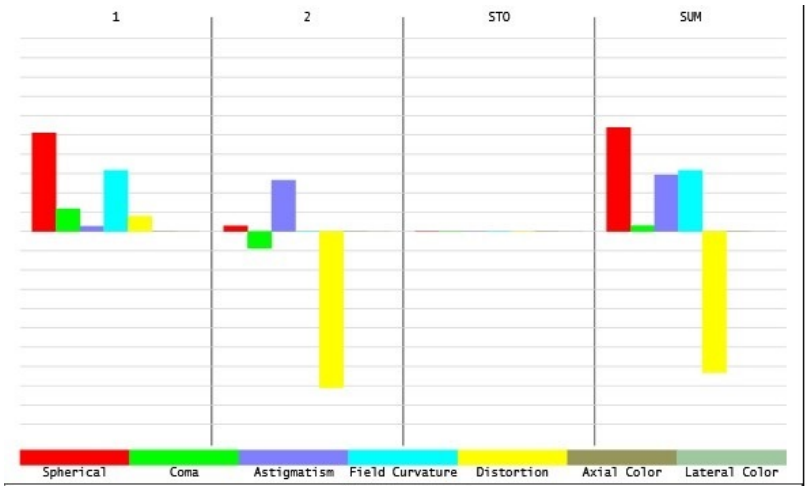

(b) Stop after optic.

Fig. 4: Seidel coefficients for lens system

2. Design of a SLR Camera Lens

Background

The goal for this section is to optimize a conventional double Gauss lens for a SLR-type camera lens. The system is to be optimized using Gaussian quadrature [1] for the F,D,C spectrum with an effective focal length of $75mm$ and $F/3$. The imaging plane is $35mm$ film and distortion must be less than 1%. The minimum edge to center distance is $2mm$ and the maximum is $12mm$ with a back focus of at least $40mm$.

The restriction of $f = 75mm$ and $h = 35mm$ means that the Angular Field of View (AFOV) for this lens should be [2],

$$AFOV(^\circ) = 2\tan^{-1}\left(\frac{h}{2f}\right) = 26.268^\circ$$

The Modulation Transfer function is desired to be above 0.5 at $30\frac{cycles}{mm}$ and above 0.2 at $50\frac{cycles}{mm}$ on axis. For a system off axis, the MTF is desired to be above .35 at $30\frac{cycles}{mm}$ and .2 at $45\frac{cycles}{mm}$

Methods

A generic file for a double Gauss lens was opened from the "Short Course" section of OpticStudio samples. The lens radii were then altered to follow the specifications for generating a double Gauss lens by sequential addition of optical components [3]. The optimization wizard was utilized to optimize for the RMS spot centroid initially with the design constraints and four additional fields. Once the system was within reasonable bounds the system was optimized for the specifications of MTF. To do this, the optimization was switched from Spot RMS to Wavefront RMS.

Results

The entire system was optimized and resulted in a set of singlets and doublets which can be seen in Fig. 5. The back focus distance is $50mm$ and the $\frac{F}{\#} = 3$ as was desired. The modulation transfer function for this design can be seen in Fig. 6 where the on axis MTF is shown on the blue curve and remains above 0.5 at $30\frac{cycles}{mm}$ and 0.2 at $50\frac{cycles}{mm}$. The distortion is shown in Fig. 7 which has a maximum distortion around 0.1% on the imaging plane which is $38x38[mm]$ which is slightly larger than desired. The field at the maximum angle is also below the distortion threshold but the MTF drops much lower than the desired off-axis ratio. There are two other off-axis fields that meet the criterion though.

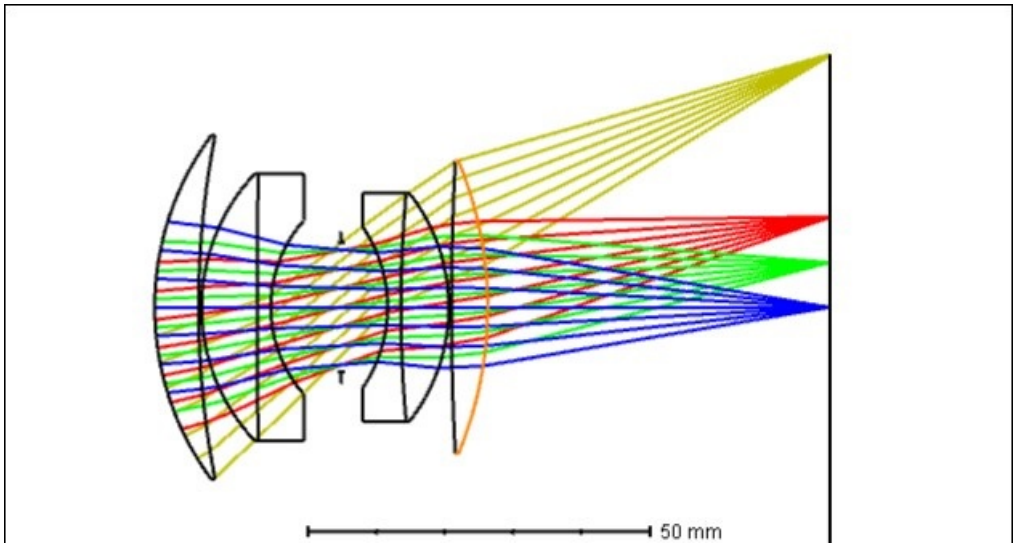

Fig. 5: Optimized Double Gauss Lens Layout

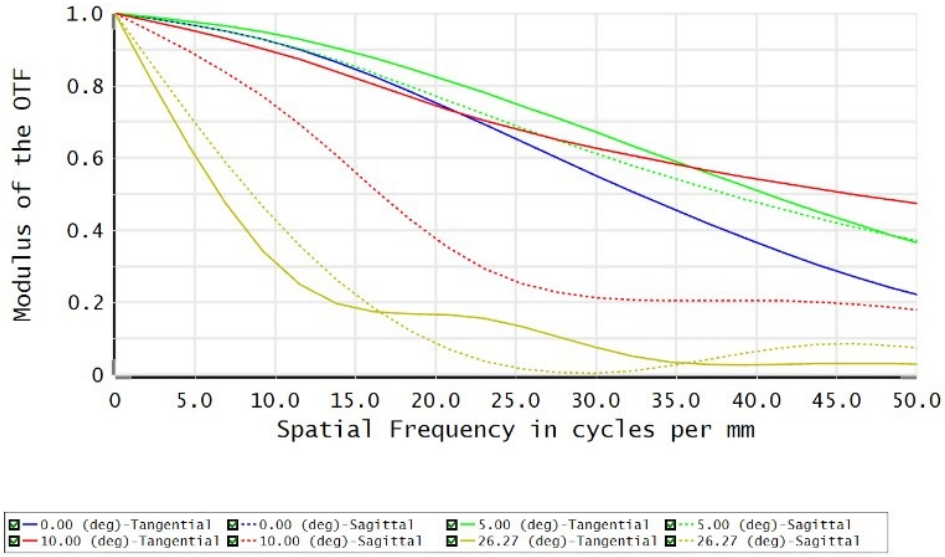

Fig. 6: Double Gauss Lens Modulation Transfer Function

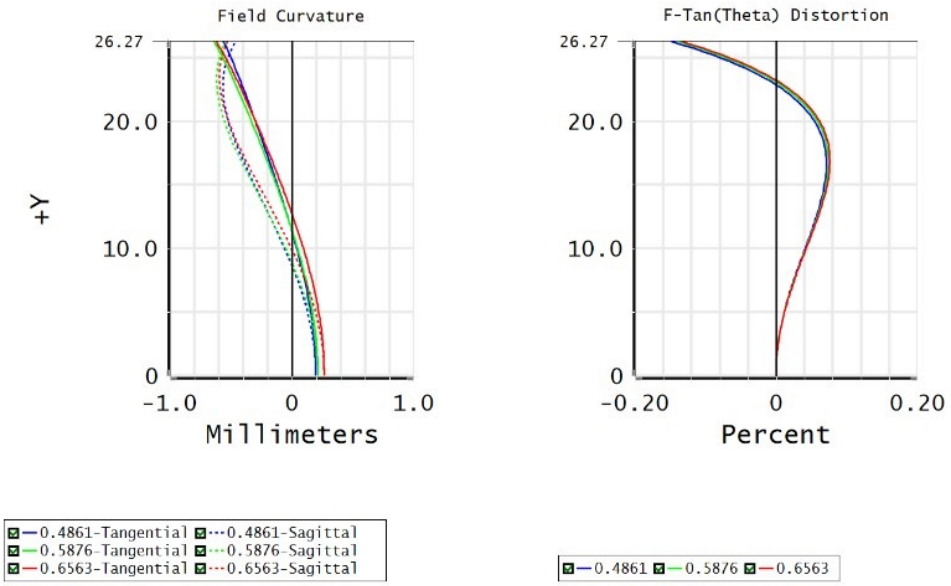

Fig. 7: Double Gauss Lens Distortion

3. Modeling Young's Double Slit

Background

The Young's double slit experiment is a classic example of the diffraction of light. The total irradiance of light that is incident on an imaging screen after having propagated through a series of slits can be found analytically with the Huygens-Fresnel principle [4], the solutions to which are:

$$I(\theta) = I_0 \left(\frac{\sin(\beta)}{\beta} \right)^2 \left(\frac{\sin(N\alpha)}{\sin(\alpha)} \right)^2 \tag{1}$$

Where the variables $\beta = \pi \lambda b \sin(\theta)$, $\alpha = \pi \lambda a \sin(\theta)$. Where the system has been assumed to be in air, θ is the angular separation from the normal, the slit width is b, slit separation is a, and wavelength of light is λ. The Young's double slit experiment is still relevant in many modern day applications such as Raman spectroscopy and Microscopy [5].

The goal here is to use OpticStudio to simulate an N-slit diffraction pattern on a screen and see how the system behaves when the wavelength, slit spacing, and slit width are varied.

Methods

An example file for a Young's double slit was downloaded [6] to simulate the experiment in OpticStudio. The coherent irradiance pattern was observed for a cross section at the center of the imaging screen with the "Detector Viewing" function. A MATLAB script was then written to plot the theoretical irradiance pattern with Eq. 1. The wavelength of light, slit separation, and slit width were varied for the double slit and the results were compared to the theoretical curves from the MATLAB script. Then the amount of slits were increased to 4 and 10 to observe the resultant irradiance patterns and they were also compared to the theory.

Results

One of the initial plots that were observed for the generic Young's double slit was the 2D intensity profile for the irradiant light on the imaging screen. These images can be seen in Fig. 8 for light at $1\mu m$ and $500nm$. While the images are quite attractive and interestingly filled with structure, it is somewhat challenging to really tell how much one image differs from the other. For that reason, the intensity profile along the x-axis of the imaging screen was chosen as the primary function of interest. One benefit of observing that particular profile is that it corresponds to the theoretical intensity profile in Eq. 1.

The first set of intensity patterns can be seen in Fig. 9a where the wavelength was set to be $1\mu m$ in and Fig. 9b where the same system was solved with a wavelength of $500nm$. The theoretical intensity profiles for the corresponding systems can be seen in Fig. 10. There are some similarities between the two images, primarily the fact that between there are the same amount of peaks and minima, and the relation of the intensities of the higher order peaks follow the same general pattern. The theoretical plots are normalized to the central peak and show a more dramatic decrease in the overall intensity at locations further from the center in comparison to those produced by OpticStudio.

In general, the intensity profiles of the double slit after the separations and widths had been changed are shown in many of the figures below. Some of the more interesting intensity profiles are the $N = 4$ and $N = 10$ which are shown in Fig. 17. There are many more lines which correspond to the convolution of the single slit with a dirac comb of size N, and the 2D color plots are shown in Fig. 15 but those are still challenging to really decipher so the intensity profiles are still preferable. The differences between the theoretical and simulated intensity profiles are mainly due to the use of finite element analysis that OpticStudio uses to ray trace.

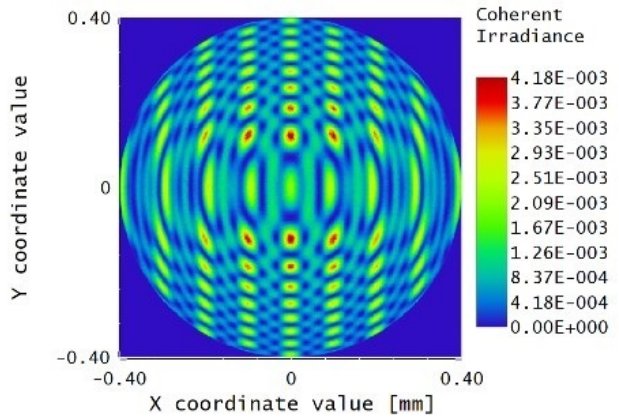

(a)

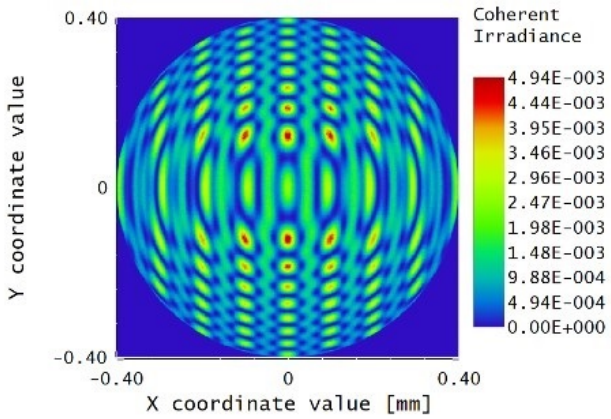

(b)

Fig. 8
Two-Dimensional Coherent Irradiance Patterns

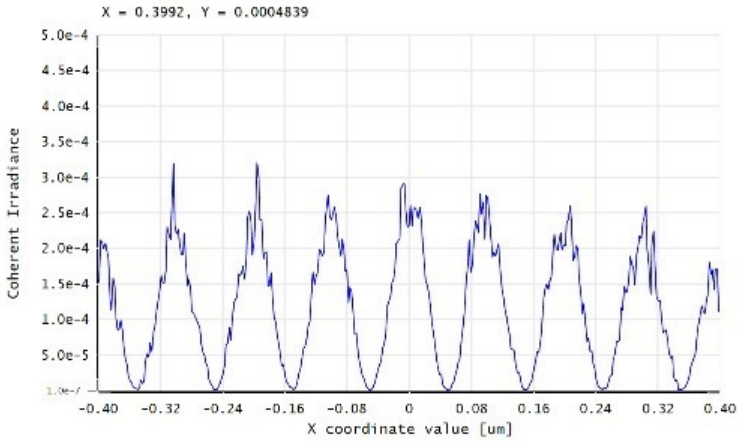

(a) $\lambda = 1\mu m$

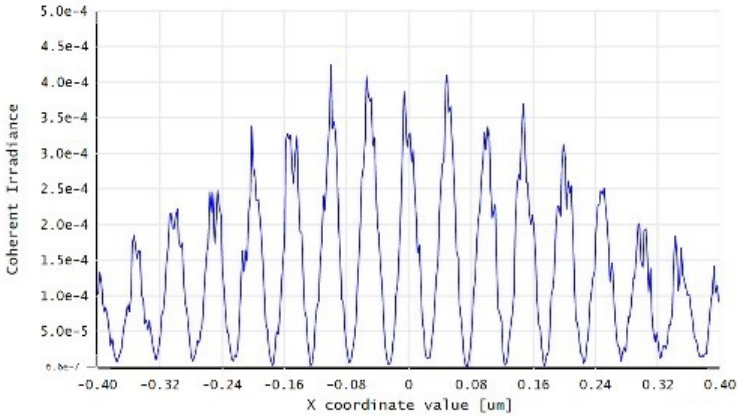

(b) $\lambda = 500nm$

Fig. 9: Intensity profiles for two different wavelengths from OpticStudio

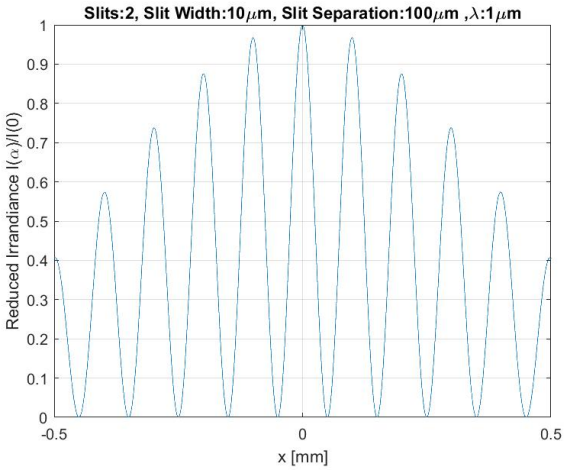

(a) $\lambda = 1\mu m$

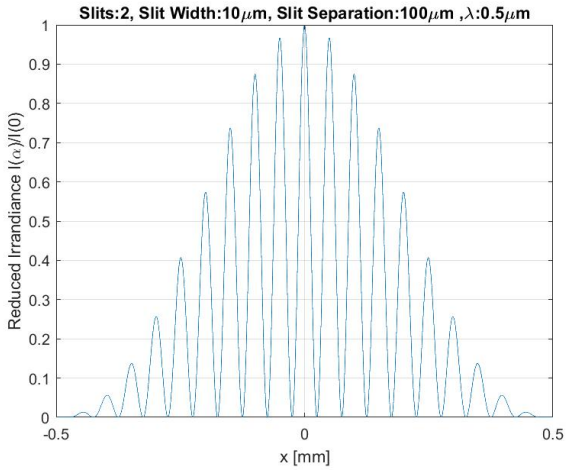

(b) $\lambda = 500nm$

Fig. 10: Corresponding intensity profiles for two different wavelengths from theory

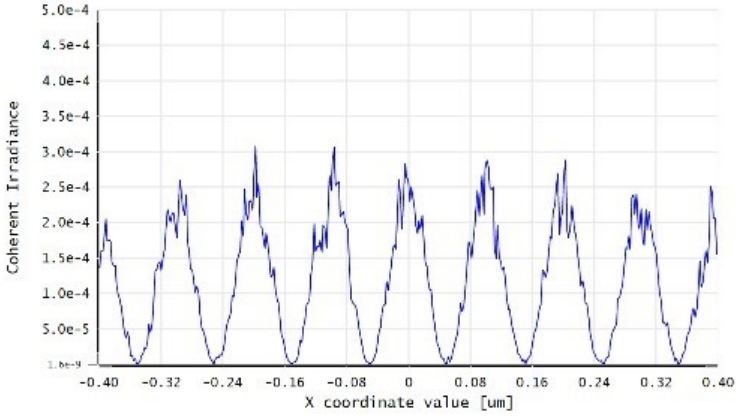

(a) Slit Width: $b = 5\mu m$, $\lambda = 1\mu m$

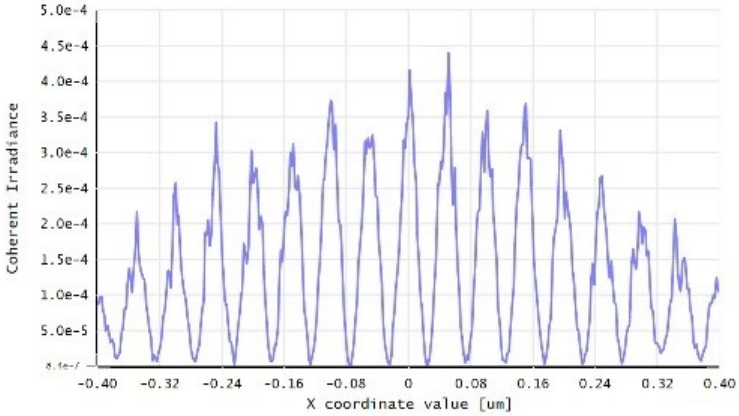

(b) Slit Width: $b = 5\mu m$, $\lambda = 500nm$

Fig. 11: OpticStudio generated intensity profiles for a $5\mu m$ slit width, in comparison to the $10\mu m$ slit width.

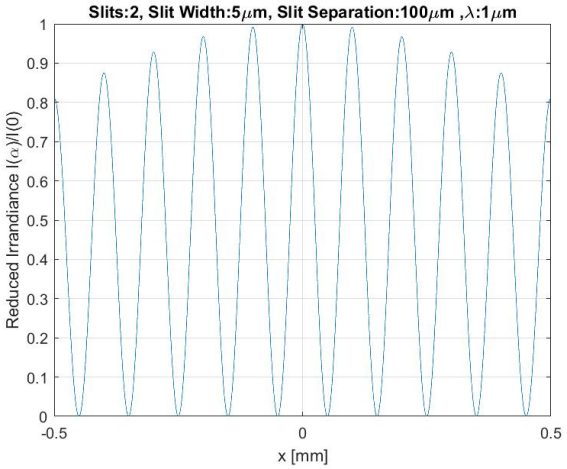

(a) Slit Width: $b = 5\mu m$, $\lambda = 1\mu m$

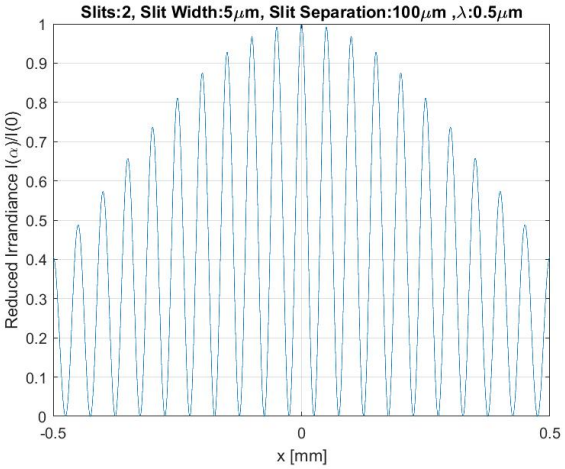

(b) Slit Width: $b = 5\mu m$, $\lambda = 500nm$

Fig. 12: Theoretical intensity profiles for a $5\mu m$ slit width.

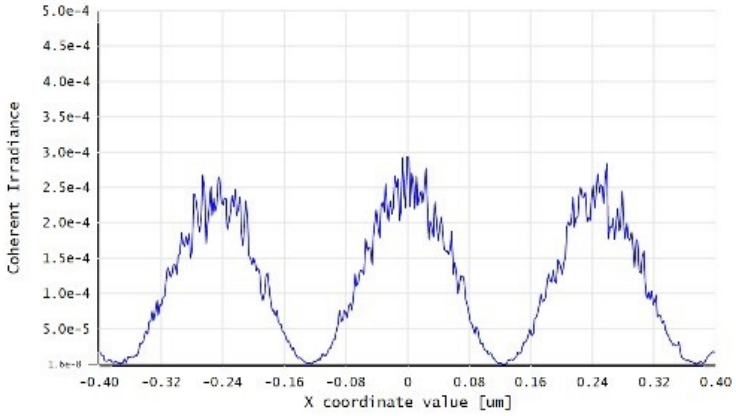

(a) Slit separation $a = 40\mu m$ for $\lambda = 1\mu m$

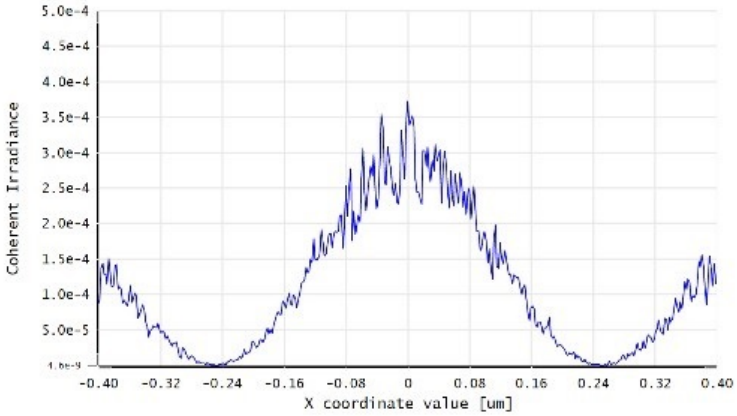

(b) Slit separation $a = 20\mu m$ for $\lambda = 1\mu m$

Fig. 13: Intensity profiles generated by OpticStudio for two different slit separations.

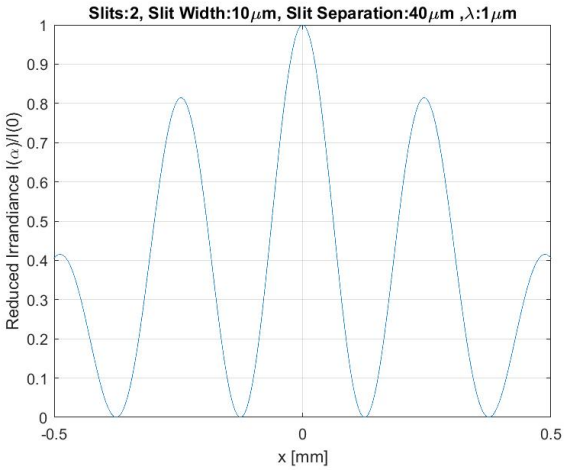

(a) Slit separation $a = 40\mu m$, $\lambda = 1\mu m$

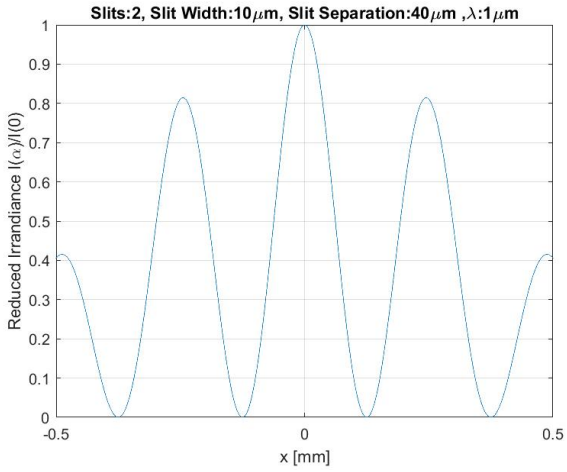

(b) Slit separation $a = 20\mu m$, $\lambda = 1\mu m$

Fig. 14: Theoretical intensity profiles for two different slit separations.

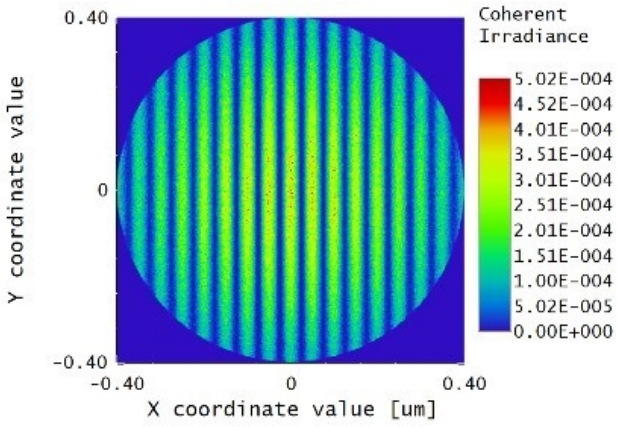

(a) N = 4 Slits

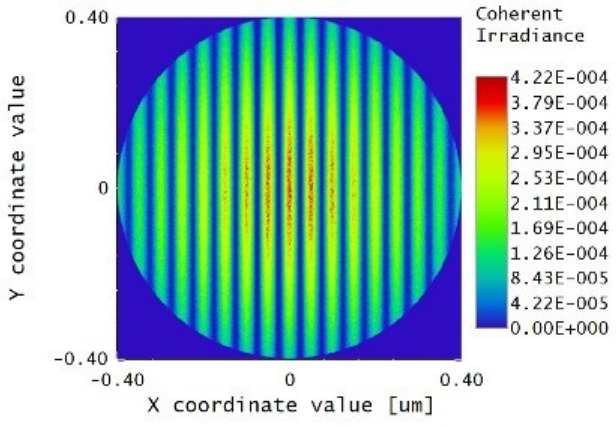

(b) N = 10 Slits

Fig. 15: Two dimensional intensity profiles

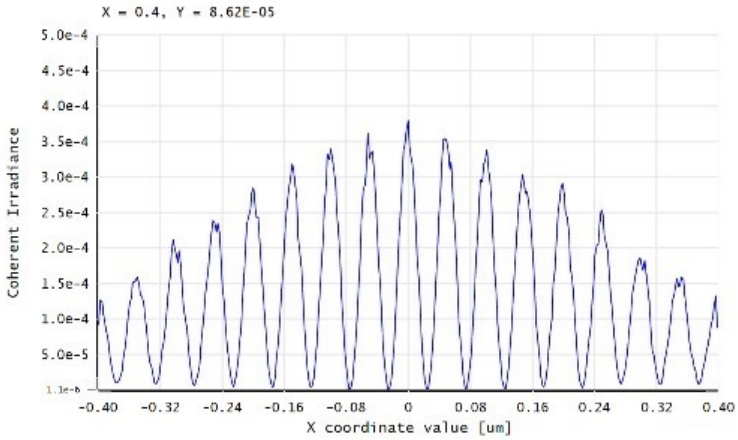

(a) N = 10

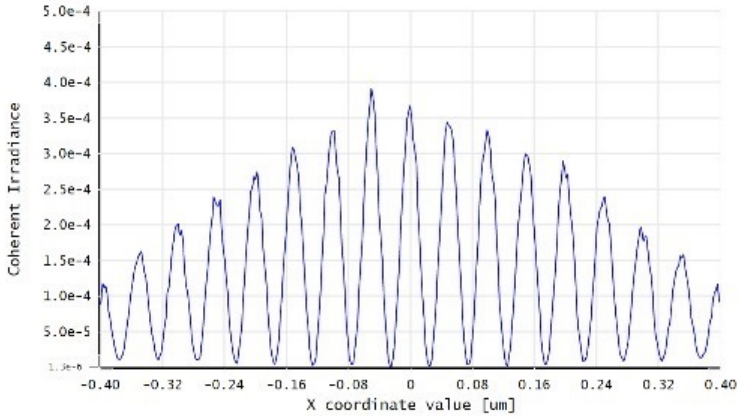

(b) N = 4

Fig. 16: N slit diffraction irradiance patterns from OpticStudio

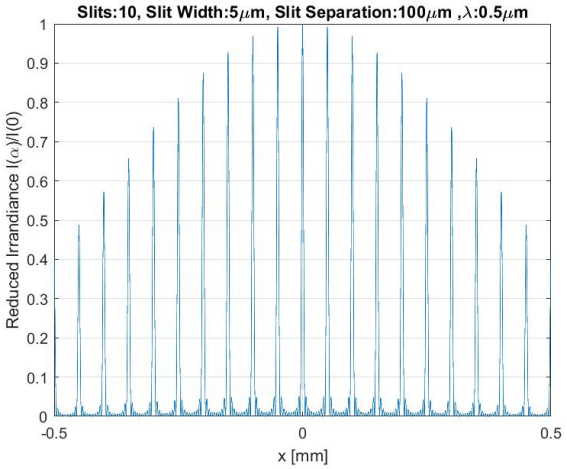

(a) N = 10

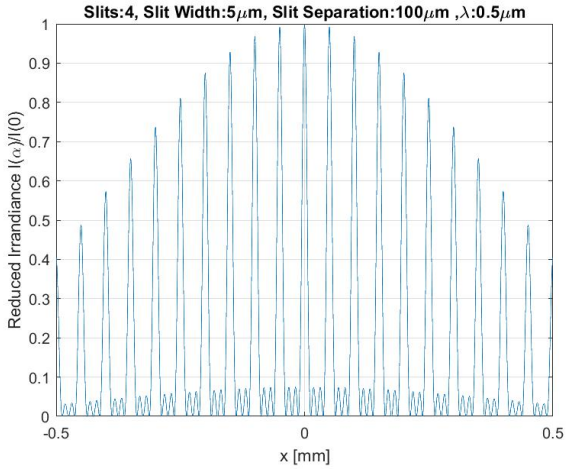

(b) N = 4

Fig. 17: Theoretical N-slit diffraction irradiance patterns.

4. Design of a Optical Spectrometer

Background

This was one of the more difficult portions to accomplish because it involved a little bit of study and creativity. It seemed to be quite popular to look for a design which was already available on the Internet, instead of following that route a design was developed from scratch. An optical spectrometer is a device which separates light into its composite wavelengths and is important for characterizing the composition of materials. The design was based off of a high resolution X-ray grating spectrometer which utilizes a variable position detector [7].

Methods

A $25mm$ aperture was used to illuminate (f,c,d) light onto a positive lens. This lens was then optimized to have a $\frac{F}{\#} = 10$ with a minimum thickness of $2mm$ and maximum $15mm$. A second lens was placed a focal length away and optimized to have the same $F/\#$ which created a collimated beam of white light. A diffraction grating was then placed $100mm$ from the back surface of the second lens and set to have a grating spacing of $1\frac{line}{\mu m}$ and diffraction order of 1.5.

The beam split into three component wavelengths corresponding the red, green, and blue. A final layer with infinite radius was placed to act as a photodetector which could potentially capture the intensity of light and develop a spectral intensity plot. In reality the photodetector would need to be mounted on a translational stage which could move about a meter in length and be able to rotate to completely capture the incident beam from the grating. This design is meant for a laboratory setting rather than manufacturing due to its size, but it could easily be scaled down.

The multi-configuration tool was used to control both the y-offset and rotation of the photodetector for the three separate wavelengths of light that arise at different locations on the imaging screen.

Results

The general spectrometer design can be seen in Fig. 18 where the three configurations are indicated by a small orange bar along the imaging plane which are labeled Pos.1-3. A better method for this type of spectrometer would be to translate the photodetector along a circumference a known distance away, but that design was somewhat challenging to perform in OpticStudio. The position of the photodetector along the imaging plane can be directly related to the wavelength of light, and a spectrum can be made. The spot diagrams for the different wavelengths of light at the three configurations of interest (Figs. 19-21) display astigmatism which would skew the overall spectrum of whatever material is being studied. This is one of the other reasons why it would be more beneficial to have a circumferentially translating photodetector whose angle of incidence wouldn't need to be altered to capture the correct amount of light for each wavelength.

5. Conclusion

Four projects were completed in OpticStudio as an exploratory introduction to the software. The first was the design of a Singlet where the position of the stop was varied in order to determine what the affects would be on the amount of aberration on the imaging plane. To determine the magnitude of aberration for the two stop positions the spot diagrams were developed for fields which were incident on the lens and at an oblique angle. The best method for determining the amount of aberrations was through the Seidel coefficients which describe the coefficients in front of the aberration functions. From these diagrams it was determined that placing the stop after the optic was better for reducing spherical aberrations, while placing the stop before the optic is better for reducing distortion and astigmatism.

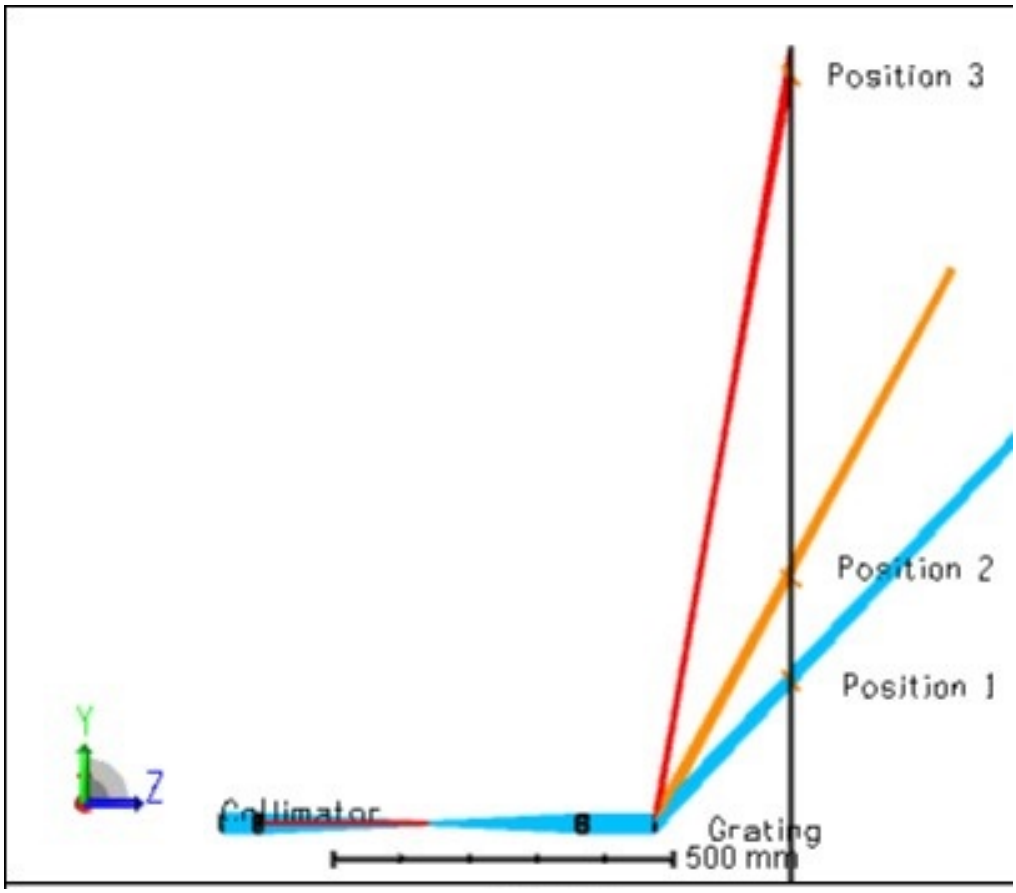

Fig. 18: Spectrometer Layout

The second endeavor was to develop and optimize a SLR-type camera lens from a Double Gauss design. A generic setup for the Double Gauss lens was opened from the samples in Zemax and the lens was then optimized to fit a set of criteria regarding the size and optical characteristics of the lens. After optimization the amount of distortion for an image was reduced to about 0.13% and the MTF for the on-axis and off-axis fields were sufficient to the design specifications.

The third portion of this lab was the most data rich, as a Young's double slit experiment was simulated for a handful of wavelengths, slit widths, and slit separations. For each of these scenarios a theoretical curve of the intensity profile was compared to the intensity profile which was solved for by OpticStudio. A set of False Color Coherent Intensity profiles were also developed but they were far too cluttered with information, so the generic intensity profiles were prioritized. In the end, the intensity profiles matched very well with the theoretical curves.

The end section revolved around the design of an Optical Spectrometer, which was simulated from scratch and based off of a simple X-ray grating diffraction spectrometer. The design used a collimated beam, incident on a diffraction grating to separate white light into its component pieces and a translational photodetector which could capture the intensity for various wavelengths.The implementation of the design was quite challenging and could be significantly improved by using the multiple configuration editor to translate planes around a circumference.

Overall this module was a moderate success, a decent amount of knowledge and confidence with OpticStudio has been gained.

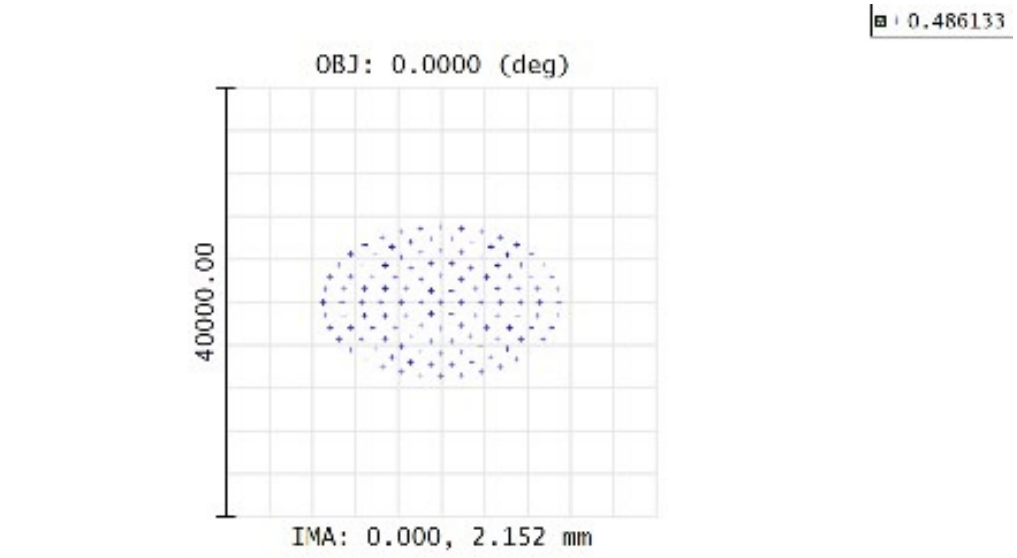

Fig. 19: Blue Light Spot Diagram

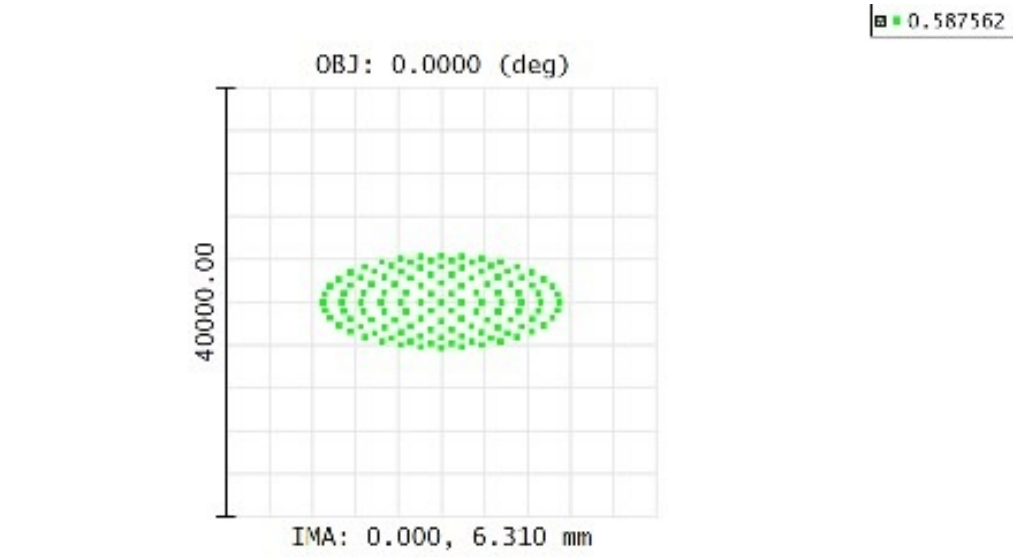

Fig. 20: Green Light Spot Diagram

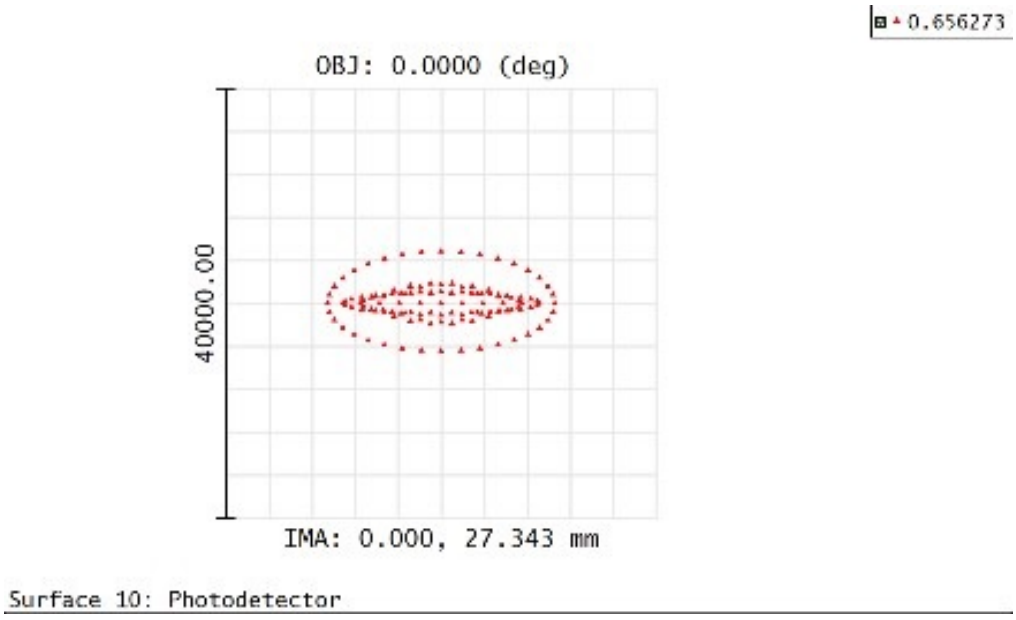

Fig. 21: Red Light Spot Diagram

References

1. S. Bakic and D. Vasiljevic, "Optimization of the double-gauss objective with the various evolution strategies and the damped least squares," Phys. Scripta **2014**, 014034 (2014).
2. E. O. Inc., "Understanding focal length and field of view," .
3. D. Shafer, "Designing a double-gauss lens, the hard way," (2017).
4. E. Hecht, "Optics, 4th," Int. edition, Addison-Wesley, San Francisco **3**, 2 (2002).
5. D. Gachet, S. Brustlein, and H. Rigneault, "Revisiting the youngâĂŹs double slit experiment for background-free nonlinear raman spectroscopy and microscopy," Phys. review letters **104**, 213905 (2010).
6. J. Wilde, "Young's pinhole interference setup simulating using ray tracing," .
7. S. Chiuzbaian and C. Hague, "High acceptance high resolution soft x-ray grating spectrometer: Choice of optical design," J. Electron Spectrosc. Relat. Phenom. **188**, 121–126 (2013).